The Astrophysical Journal, 728:43 (9pp), 2011 February 10 doi:10.1088/0004-637X/728/1/43

THE ABUNDANCES OF POLYACETYLENES TOWARD CRL618

J. P. Fonfría[1], J. Cernicharo[2], M. J. Richter[3,5], and J. H. Lacy[4,5]

[1] Departamento de Estrellas y Medio Interestelar, Instituto de Astronomía, UNAM, Ciudad Universitaria, 04510, Mexico City, Mexico; fonfria@astroscu.unam.mx

[2] Laboratorio de Astrofísica Molecular, Departamento de Astrofísica, Centro de Astrobiología, INTA, 28850 Torrejón de Ardoz, Madrid, Spain; cerni@damir.iem.csic.es

[3] Physics Department—UC Davis, One Shields Ave., Davis, CA 95616, USA; richter@physics.ucdavis.edu

[4] Astronomy Department, University of Texas, Austin, TX 78712, USA; lacy@shrub.as.utexas.edu

Received 2010 April 12; accepted 2010 November 30; published 2011 January 18

ABSTRACT

We present a mid-infrared high spectral resolution spectrum of CRL618 in the frequency ranges 778–784 and 1227–1249 cm^{-1} (8.01–8.15 and 12.75–12.85 μm) taken with the Texas Echelon-cross-Echelle Spectrograph (TEXES) and the Infrared Telescope Facility (IRTF). We have identified more than 170 rovibrational lines arising from C_2H_2, HCN, C_4H_2, and C_6H_2. We have found no unmistakable trace of C_8H_2. The line profiles display a complex structure suggesting the presence of polyacetylenes in several components of the circumstellar envelope (CSE). We derive total column densities of 2.5×10^{17}, 3.1×10^{17}, 2.1×10^{17}, 9.3×10^{16} cm^{-2}, and $\lesssim 5 \times 10^{16}$ cm^{-2} for HCN, C_2H_2, C_4H_2, C_6H_2, and C_8H_2, respectively. The observations indicate that both the rotational and vibrational temperatures in the innermost CSE depend on the molecule, varying from 100 to 350 K for the rotational temperatures and 100 to 500 K for the vibrational temperatures. Our results support a chemistry in the innermost CSE based on radical-neutral reactions triggered by the intense UV radiation field.

Key words: line: identification – line: profiles – stars: AGB and post-AGB – stars: carbon – stars: individual (CRL618) – surveys

Online-only material: color figures

1. INTRODUCTION

The protoplanetary nebula (PPN) stage is one of the shortest of a sun-like star's evolution (e.g., Iben & Renzini 1983). Throughout this phase, roughly half of the stellar photosphere is ejected, shocking the gas of the circumstellar envelope (CSE) formed in the asymptotic giant branch (AGB) stage (AGB–CSE; Kwok et al. 1978), and unveiling the outermost layers of the nucleus. The stellar UV radiation field is extremely intense in this phase, photodissociating the innermost circumstellar gas and triggering a particularly rich photochemistry (Woods et al. 2002, 2003; Redman et al. 2003; Cernicharo 2004, hereafter C04).

CRL618 (Westbrook Nebula, AFGL 618) is a very young PPN (age $\simeq$ 200 yr; Kwok & Bignell 1984), located at a distance of $\simeq$0.9–1.8 kpc from the Sun (Schmidt & Cohen 1981; Goodrich 1991; Knapp et al. 1993; Sánchez-Contreras & Sahai 2004). It contains a B0 central star embedded in a dusty ultracompact H II region surrounded by a torus and a low-velocity expanding envelope with an external radius $>20''$, a total mass $\simeq 1\,M_\odot$, and an expansion velocity $v_{exp} \simeq$ 18.0–21.5 km s^{-1} (Knapp & Morris 1985; Fuente et al. 1998; Pardo et al. 2004). In addition, it displays gas with velocities as high as 200 km s^{-1} (Burton & Geballe 1986; Cernicharo et al. 1989; Gammie et al. 1989). This high velocity gas (HVG) is the molecular counterpart of the bright optical jets oriented in the E–W direction (Trammell 2000) which impact the AGB–CSE and produce the well-known optical lobes.

Since its discovery by Westbrook et al. (1975), many molecular species have been detected toward this PPN (Cernicharo et al. 1989, 2001a, 2001b; Herpin & Cernicharo 2000; Remijan et al. 2005; Truong-Bach et al. 1996), some of them for the first time in a C-rich CSE (e.g., formaldehyde, polyacetylenes C_4H_2 and C_6H_2, benzene, H_2O and OH; Cernicharo et al. 1989, 2001a, 2001b; Herpin & Cernicharo 2000). The CSE developed in the AGB phase has been studied in great detail by several authors (see, e.g., Cernicharo et al. 2001a, 2001b; Sánchez-Contreras & Sahai 2004; Sánchez-Contreras et al. 2004; Pardo et al. 2004, 2005; Pardo & Cernicharo 2007; Pardo et al. 2007, and references therein).

Woods et al. (2003, hereafter W03) and C04 have modeled the chemistry of CRL618 suggesting that in the innermost envelope, the UV photons photodissociate C_2H_2 producing the radical C_2H, which can react with C_2H_2 to form C_4H_2 or with H_2 reforming C_2H_2. Additionally, C_2H can react with C_4H_2 forming C_6H_2. These processes lead to a rapid C_2H_2 polymerization in long carbon chains and clusters. The abundance ratio between consecutive polyacetylenes ($C_{2n}H_2$, $n = 1, 2, 3, \ldots$) in CRL618 has been estimated as a factor of $\simeq$2–3 (Cernicharo et al. 2001b, hereafter C01b). Polyacetylenes are symmetric molecules without a permanent dipole moment and, hence, detectable only through their rovibrational spectra. The strongest bands of their spectra are expected to fall in the mid-infrared range due to the physical conditions prevailing in the innermost CSE where the polyacetylenes are built up. However, the large telluric opacity in the infrared has largely prevented the exploitation of this frequency range. This issue has been overcome with the launch of the *Infrared Space Observatory* (*ISO*) and the *Spitzer Space Telescope*, and the development of instruments with high spectral resolving power such as the Texas Echelon-cross-Echelle Spectrograph (TEXES; Lacy et al. 2002). The analysis of these kinds of observations will allow us to improve our knowledge about the polymerization processes and the formation of complex molecules such as long carbon chains, polycyclic aromatic hydrocarbons (PAHs), and

[5] Visiting Astronomer at the Infrared Telescope Facility, which is operated by the University of Hawaii under contract from the National Aeronautics and Space Administration.

fullerenes (C_{60} and C_{70}), which have been recently observed toward circumstellar and interstellar environments (Cami et al. 2010; García-Hernández et al. 2010; Sellgren et al. 2010) and whose ions could be the carriers of the diffuse interstellar bands (DIBs; Foing & Ehrenfreund 1994).

In this paper, we present a high-resolution mid-infrared spectrum of CRL618. We have identified ≃170 rovibrational lines of bands $\nu_6 + \nu_8$, $\nu_6 + \nu_8 + \nu_9 - \nu_9$, $\nu_6 + \nu_8 + 2\nu_9 - 2\nu_9$, and $\nu_6 + \nu_8 + \nu_7 - \nu_7$ of C_4H_2, and $\nu_8 + \nu_{11}$ of C_6H_2. In addition, we have observed several lines of C_2H_2 and HCN. These lines have been analyzed by using a modified version of the model of AGB envelopes developed by Fonfría et al. (2008, hereafter F08). The observations and the spectroscopic laboratory data of HCN and polyacetylenes required to analyze the observations are presented in Sections 2 and 3, respectively. A description of the spectrum and the model, the adopted fitting strategy, and a discussion about the uncertainties of the parameters can be found in Section 4. The results derived from our fits are presented and discussed in Section 5 and, finally, summarized in Section 6.

2. OBSERVATIONS

We observed CRL618 using the TEXES spectrograph (Lacy et al. 2002) on the IRTF 3 m telescope during the first half of the nights of 2002 December 12 and 2004 January 8. TEXES was used in high spectral resolution mode which gives $R \simeq 10^5$. Six separate settings were used to cover from 778 to 784 cm^{-1} (2002 December 12) and 1205 to 1250 cm^{-1} (2004 January 8; see Figure 1). For each setting, the Becklin–Neugebauer (BN) object (Becklin & Neugebauer 1967) was observed as a telluric reference before changing the instrumental setup. To date, TEXES has detected no spectral features in BN at these wavelengths. The spectrograph slit was roughly 1.″4 wide for all observations. The spectral coverage and slit length varied depending on the setting. The slit was always long enough that we nodded along the slit every 16 s to remove background emission.

The data were processed using the TEXES data reduction pipeline (Lacy et al. 2002). The pipeline operates on the raw data files and produces optimally extracted, one-dimensional spectra with a frequency scale set by user identification of atmospheric lines. Using the difference of an ambient temperature blackbody and the night sky emission, it is possible to correct partially for telluric spectral features. Additional correction comes from comparison with the telluric standard. The baseline has been removed by using fourth-order polynomials. The range 1205–1227 cm^{-1} shows a ripple whose period is roughly twice the observed line widths and that would severely compromise analysis of any line in this range. Hence, this range has not been analyzed.

A realistic modeling of molecular lines requires an estimation of the dust emission throughout the envelope. It provides us with an estimation of the dust opacity and temperature in different shells, allowing us to determine how it affects the molecular emission. Since the infrared continuum of CRL618 has remained roughly constant for several decades (Kleinmann et al. 1978; Pottasch et al. 1984; C01b), we have supplemented the TEXES/IRTF data with a low-resolution Short-wavelength Spectrometer (SWS)/*ISO* spectrum (C01b) covering the range between 2.4 and 45 μm. The properties of the dusty CSE derived from modeling this continuum will be subsequently used to calculate the synthetic profiles of the molecular lines (see Section 4).

3. SPECTROSCOPIC DATA

All the molecular species considered in this work (HCN, C_2H_2, C_4H_2, C_6H_2, and maybe C_8H_2) are linear. The frequencies and intensities of the lines of C_2H_2 and HCN have been extensively studied in the laboratory but those of C_4H_2, C_6H_2, and C_8H_2 are still not accurately measured. The frequencies of the rovibrational transitions of the bands observed in our spectrum are well known in the case of C_4H_2 and C_6H_2. However, the rovibrational spectrum of C_8H_2 remains unknown (Shindo et al. 2001).

C_4H_2 is a six-atom linear molecule with nine vibrational modes. Four of them (ν_6–ν_9) are doubly degenerated bending modes with energies of 625.4986, 482.7078, 627.8958, and 219.9778 cm^{-1}. The rotational constant in the ground vibrational state is 0.1464102 cm^{-1} (Guelachvili et al. 1984). The spectroscopic constants have been taken from Guelachvili et al. (1984), McNaughton & Bruget (1992), Arié et al. (1992), and Matsumura & Tanaka (1982, 1984). The measured band intensity is ≃171 cm^{-2} atm^{-1} (Khlifi et al. 1995), implying that the derived dipole moments of the rovibrational transitions of band $\nu_6 + \nu_8$ are ≃0.096 D.

C_6H_2 is an eight-atom molecule with 13 vibrational modes; the last six (ν_8–ν_{13}) are doubly degenerated bending modes. Their energies are 622.38, 491.00, 258.00, 621.34, 443.50, and 105.04 cm^{-1}. The rotational constant in the ground vibrational state is 0.044171 cm^{-1}. All these data and the rest of the spectroscopic constants have been taken from Matsumura et al. (1993), McNaughton & Bruget (1991), and Haas et al. (1994). The dipole moments of the rovibrational transitions of band $\nu_8 + \nu_{11}$ are ≃0.12 D, derived from a band intensity ≃210 cm^{-2} atm^{-1} (Shindo et al. 2003).

The central frequency of the $C_8H_2\nu_{10} + \nu_{14}$ band is not accurately known but it is expected to fall inside the observed range at ≃1230 cm^{-1}. It has a small ground rotational constant, ≃2×10^{-2} cm^{-1} (Shindo et al. 2001), which will produce a band formed by a series of lines partially resolved with the resolution power provided by TEXES, and a FWHM ≃5 cm^{-1} at the temperatures prevailing in the innermost CSE of CRL618. This structure could be easily identified, if the abundance of this species is large enough to produce absorption above 10% of the continuum, in view of the large density of lines from the other species. The estimated dipole moment of this band is ≃0.14 D, which has been derived from the band intensity ≃256 cm^{-2} atm^{-1} (Shindo et al. 2001).

For these three molecules (C_4H_2, C_6H_2, and C_8H_2), only the intensities of the whole bands are available in the literature. It is worth noting that the observed bands are blended with several hot bands (e.g., for C_4H_2 the observed band is $\nu_6 + \nu_8$ and the associated hot bands are $\nu_6 + \nu_8 + \nu_9 - \nu_9$, $\nu_6 + \nu_8 + 2\nu_9 - 2\nu_9$, ...) involving vibrational states significantly populated at room temperature. Therefore, we have estimated the dipole moment of the rovibrational transitions of the fundamental band of each molecule from the intensity measurements quoted in the literature and we have assumed that the hot bands ($\nu_6+\nu_8+\nu_9-\nu_9$, $\nu_6 + \nu_8 + 2\nu_9 - 2\nu_9$, ...) have the same dipole moment as the $\nu_6 + \nu_8$ one. The consequences of this approximation will be discussed in Section 4.1.

The frequencies and dipole moments of C_2H_2 and HCN have been taken from the HITRAN database (Rothman et al. 2005).

Several bands from ^{13}C-bearing isotopologues of HCN and the polyacetylenes are expected to fall in the observed frequency ranges. Pardo & Cernicharo (2007) suggested a

$^{12}C/^{13}C$ ratio $\simeq$15 in the torus, meaning that [HCN]/[$H^{13}CN$] $\simeq$ 15 and [C_2H_2]/[$H^{13}CCH$] $\simeq$ [C_4H_2]/[$H^{13}CCCCH$] $\simeq$ [C_4H_2]/[$HC^{13}CCCH$] $\simeq$ 7.5, where $H^{13}CN$, $H^{13}CCH$, $H^{13}CCCCH$, and $HC^{13}CCCH$ are the most abundant isotopologues after the main ones. The HCN lines present in the observed spectrum are too weak to expect a detectable absorption from $H^{13}CN$ (Figure 1(a)). Concerning acetylene, although $H^{13}CCH$ lines might be assigned to several very weak features (Figure 1(a)), their opacities are too low to affect the much stronger C_2H_2 and HCN lines or to be used to derive any reliable information about $H^{13}CCH$. There is almost no information about the isotopologues of C_4H_2 in the literature. The center of the bands have been estimated from ab initio calculations to be shifted between 5 and 10 cm^{-1} from that of the main isotopologue (McNaughton & Bruget 1992), but these values could be affected by large uncertainties. All the significant features in the frequency range 1228–1249 cm^{-1} of the observed spectrum can be explained by considering just C_4H_2 and C_6H_2 (Figures 1(b) and (c)). Therefore, either the bands of the isotopologues actually fall out of the observed frequency range or their abundances are insufficient to produce detectable lines.

4. DESCRIPTION OF THE SPECTRA AND MODELING

The broad continuum of CRL618 taken with SWS/*ISO* displays the maximum emission at $\simeq$40 μm, typical of a cold envelope (see Figure 2). The spectrum shows solid state bands, although much weaker than those displayed in the continuum of the C-rich AGB star IRC+10216, where the bands due to solid SiC at 11 μm and that at 27 μm (whose carrier is still unknown but usually assigned to MgS; e.g., Hony et al. 2002) are clearly present (Cernicharo et al. 1999). Despite the complex geometry found in the CSE of CRL618 (see Section 1), the broad continuum emission from the dust grains smoothes any geometrical effect in the spectrum. Therefore, the dusty AGB–CSE can be assumed to be spherically symmetric in a first approximation. We have used the model of the CSE developed by F08 and assumed that the dust grains are composed of amorphous carbon (Rouleau & Martin 1991) to fit the continuum between 6 and 45 μm. To date, this model cannot deal with radiative scattering by dust grains. Hence, we limit our fitting to wavelengths above 6 μm. The central source has been assumed to have an angular size $\alpha_c \simeq 0\farcs135$ (Pardo et al. 2004, 2007), which was determined from a high-quality modeling of a large set of HC_3N lines in the millimetric range. We have adopted a distance to the source of 900 pc, derived from the luminosity–distance relationship for PPNe and estimations of the proper motion of dense inhomogeneities in the high velocity lobes (Goodrich 1991; Sánchez-Contreras & Sahai 2004). These data imply a linear radius for the continuum source $R_c \simeq 1.8\times10^{15}$ cm. The CSE is assumed to have a radius of 600 α_c, since the model displays no significant contribution to the flux from gas and dust located at larger radii. We have chosen a dust temperature following an $r^{-\gamma_d}$ law with different values for the exponent in the torus and the AGB–CSE. The exponent γ_d has been assumed to be $\simeq$0.39 over the latter region as in the case of IRC+10216 (F08; Sopka et al. 1985). The synthetic spectrum has been fit to the data by eye, the best-fitting strategy when features such as solid state bands, which cannot usually be well reproduced with current laboratory or theoretical data, are present. The parameters derived following this procedure are shown in Table 1. The largest differences between the synthetic and the observed spectra come from the C_2H_2 and HCN bands at 13 μm and the solid state features between 20 and 40 μm which are not considered in the fit (Figure 2). A discussion about the sensitivity of the synthetic spectrum to variations in the parameters presented above can be found in Section 4.1.

Table 1
Derived Parameters

Parameter	Units	Value	Errors
N(HCN)	cm^{-2}	$(2.5\pm0.9)\times10^{17}$	(6)
N(C_2H_2)	cm^{-2}	$(3.1\pm0.7)\times10^{17}$	(2)
N(C_4H_2)	cm^{-2}	$(2.1\pm0.3)\times10^{17}$	(3, 4)
N(C_6H_2)	cm^{-2}	$(9.3\pm1.4)\times10^{16}$	(5)
$v_{exp}(R_c)$	km s^{-1}	$1.00^{+0.40}_{-0.22}$	(2)
$v_{exp}(R_{d1})$	km s^{-1}	$8.00^{+0.20}_{-0.50}$	(2)
$v_{exp}(R_{d2})$	km s^{-1}	17.0 $\pm$ 0.8	(2)
R_{d3}	R_c	11.0 $\pm$ 1.0	(1)
T_{rot}(HCN)	K	350 $\pm$ 50	(6)
T_{rot}(C_2H_2)	K	200 $\pm$ 20	(2)
T_{rot}(C_4H_2)	K	100 $\pm$ 20	(3)
T_{rot}(C_6H_2)	K	100^{+100}_{-80}	(5)
T_c	K	400 $\pm$ 50	(1)
$T_d(R_c)$	K	110 $\pm$ 6	(1)
$T_d(R_{d3})$	K	98 $\pm$ 4	(1)
τ_d(8 μm)		2.3 $\pm$ 0.3	(1)
ξ_{torus}	%	65^{+12}_{-18}	(1)
ξ_{AGB}	%	35 $\pm$ 5	(1)

Notes. N(X): total column density of species X; $v_{exp}(r)$: gas expansion velocity at radius r; R_{d3}: radius of the outer boundary of the torus; $T_{rot}(X)$: rotational temperature of species X at the inner boundary of the torus; T_c: blackbody temperature of the central source; $T_d(r)$: dust temperature at radius r; τ_d(8 μm): dust optical depth at 8 μm; ξ_{torus} and ξ_{AGB}: fractions of the total dust optical depth coming from the torus and the AGB–CSE, respectively. The uncertainties have been calculated by varying the parameters related to (1) continuum, (2) C_2H_2 $\nu_5 R_e(21)$, (3) C_4H_2 $\nu_6+\nu_8 R_e(7)$, (4) C_4H_2 $\nu_6+\nu_8 R_e(22)$, (5) C_6H_2 $\nu_8+\nu_{11} R_e(34)$, and (6) HCN $\nu_2 R_e(22)$. N(C_2H_2) and N(HCN) have been estimated from the CSE and the HVG at once. See Section 5 for separate estimations in each structure. In the calculations, we have assumed the distance to CRL618 and the size of the central source as fixed. See the text (Section 4.1) for a deeper explanation about the strategy followed for the estimation of the uncertainties.

We estimate the rms noise of the TEXES/IRTF spectrum to be $\sigma \simeq 1\%$. With this noise level, we assume that a line is detected if its absorption and/or emission is larger than 3σ. The part of the spectrum ranging from 778 to 784 cm^{-1} shows three C_2H_2 lines from band ν_5 and two HCN lines from band ν_2. However, there are some features in the spectrum that do not fulfill the 3σ condition but might be assigned to transitions of the C_2H_2 bands $\nu_4+\nu_5-\nu_4$ and $2\nu_5-\nu_5$. The strongest line in this range is C_2H_2 $\nu_5 R_e(21)$. The range between 1228 and 1249 cm^{-1} shows C_4H_2 lines from the fundamental band $\nu_6+\nu_8$ and the hot bands $\nu_6+\nu_8+\nu_9-\nu_9$, $\nu_6+\nu_8+2\nu_9-2\nu_9$, and (maybe) $\nu_6+\nu_8+\nu_7-\nu_7$ (rovibrational constants for these bands are from McNaughton & Bruget 1992). The $\nu_8+\nu_{11}$ band of C_6H_2 appears as weak lines often overlapped with those of the C_4H_2 $\nu_6+\nu_8 P_e$ branch (Figures 1 and 3).

Both C_2H_2 ν_5 and C_4H_2 $\nu_6+\nu_8$ lines are broad (FWHM $\simeq$ 35 and 20 km s^{-1} with a spectral resolution of $\simeq$4 km s^{-1}), in contrast with those of the hot bands ($\simeq$10 km s^{-1}; Figure 3). The profiles of the lines of these fundamental bands exhibit a main absorption surrounded by several features at lower and higher frequencies. Some of these features are associated with hot bands and with C_6H_2 lines from the fundamental band $\nu_8+\nu_{11}$ (Figure 3). Pardo et al. (2004, hereafter P04) suggest a constant turbulence velocity in the torus $\simeq$3.5 km s^{-1} and an expansion

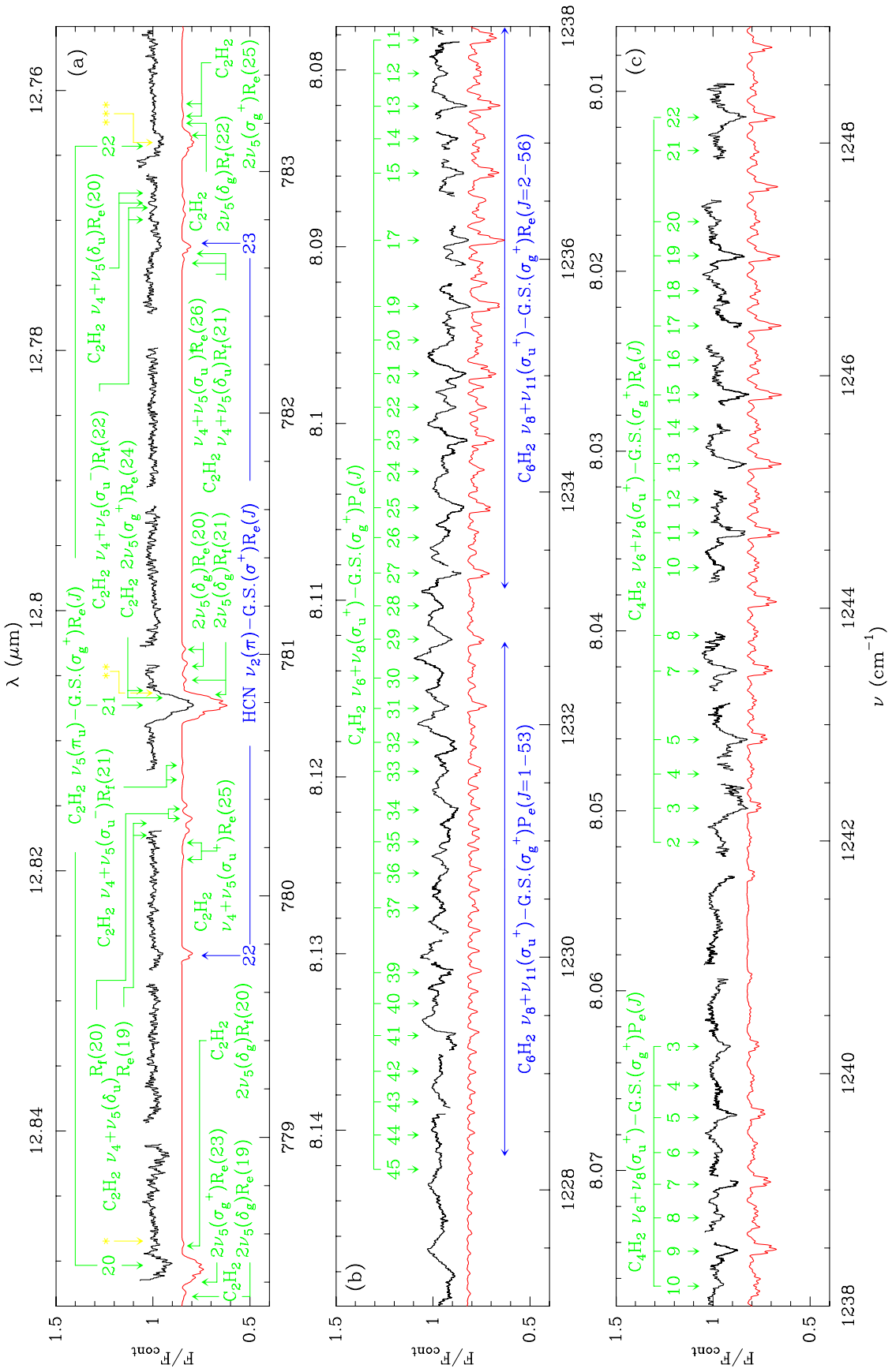

Figure 1. Observed and synthetic spectra toward CRL618 (black and red). (a) Spectra in the range 778–784 cm^{-1}. The detected lines are produced by C_2H_2 and HCN (green and blue). The asterisks (yellow) indicate several absorptions that could be assigned to the $H^{13}CCH$ lines $\nu_5 R_e(21)$, $R_e(22)$, and $R_e(23)$ (*, **, and ***, respectively). (b) and (c) Spectra ranging from 1227 to 1249 cm^{-1} contain C_4H_2 $\nu_6 + \nu_8$ and C_6H_2 $\nu_8 + \nu_{11}$ bands (green and blue). See the text for the modeling details of these lines.

(A color version of this figure is available in the online journal.)

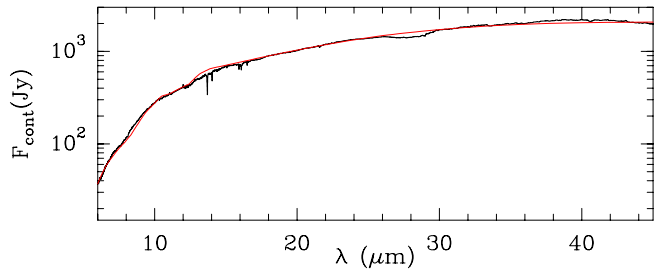

Figure 2. Observed continuum of CRL618 (SWS/*ISO*; black) and fit between 6 and 45 μm (red). A broad feature can be seen at $\simeq$28 μm, which can be assigned to the solid state band produced by the unknown material usually assumed to be MgS. The fit has been calculated by assuming dust grains composed of amorphous carbon (see the text for details).

(A color version of this figure is available in the online journal.)

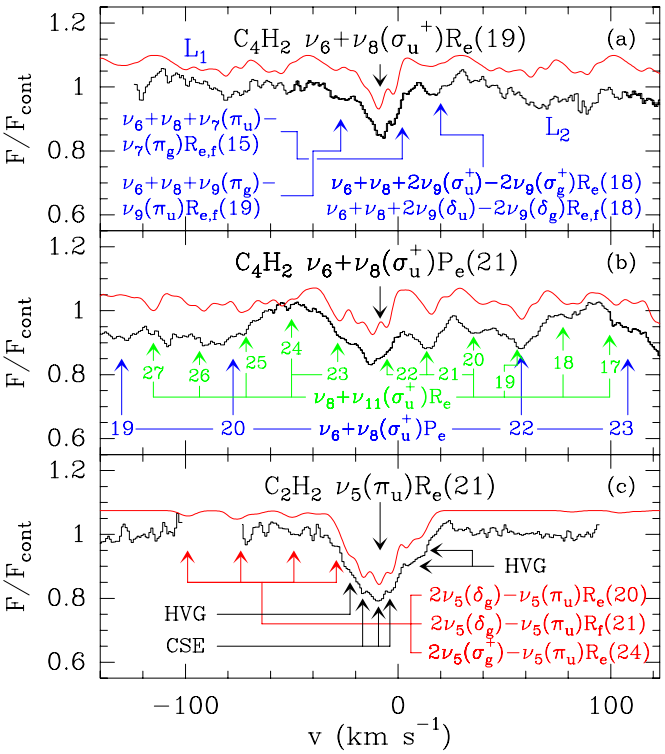

Figure 3. Comparison between observed and synthetic C_2H_2 and C_4H_2 lines. The strongest lines are (a) C_4H_2 $\nu_6+\nu_8(\sigma_u^+)R_e(19)$, (b) C_4H_2 $\nu_6+\nu_8(\sigma_u^+)P_e(21)$, and (c) C_2H_2 $\nu_5(\pi_u)R_e(21)$. These spectra show additional C_4H_2 and C_6H_2 lines (panel (a): L_1 and L_2 are C_4H_2 $\nu_6+\nu_8(\sigma_u^+)R_e(20)$ and $R_e(18)$; panel (b): C_4H_2 in blue and C_6H_2 in green). The velocity axis is centered in the LSR systemic velocity ($\simeq -21.3$ km s^{-1}; Pardo et al. 2004). The maximum absorptions in the strongest lines arise from the CSE, displaying velocities of $\simeq -3.5$, -9.0, and -16.0 km s^{-1}. The C_2H_2 line (panel c) shows the HVG contribution. These features are not present in the C_4H_2 lines implying that they arise just from the CSE.

(A color version of this figure is available in the online journal.)

velocity $\lesssim$18 km s^{-1}, allowing many of the unassigned features within the line profiles to be attributed to C_4H_2 and C_2H_2 expanding in this region. However, the origin of the remaining C_2H_2 line features is less certain since they require expansion velocities significantly larger than that observed in the torus (see Figure 3). We estimate from our model that the emission from the central source at 8 μm is at least five orders of magnitude larger than that coming from regions with an impact parameter $b > \alpha_c$. Hence, these unexplained features could arise from the gas in the HVG located in front of the central source (P04; Sánchez-Contreras & Sahai 2004).

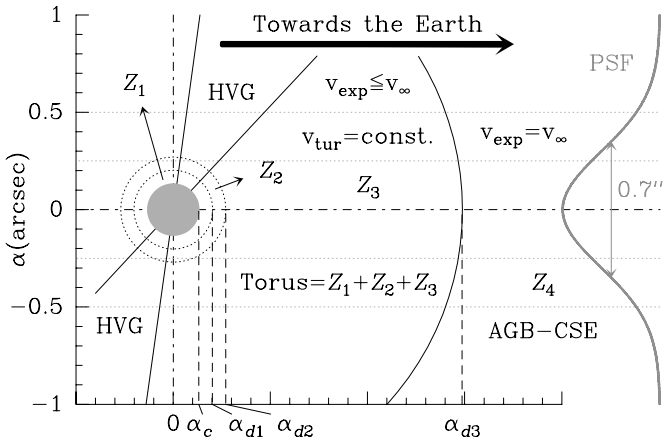

Figure 4. Model of the inner envelope of CRL618. The CSE is composed of four shells: $\mathcal{Z}_1$, $\mathcal{Z}_2$, and $\mathcal{Z}_3$ inside the torus, and $\mathcal{Z}_4$ corresponding to the AGB–CSE. We have adopted an angular radius for the central source $\alpha_c \simeq 0\farcs135$ (P04). The values of the angular radii α_{d1} and α_{d2} are assumed to be $1.5\alpha_c$ and $2.0\alpha_c$, respectively, to allow the model to deal with unexpected sharp variations of the physical conditions. The radius α_{d3} has been considered a free parameter. We have assumed a constant turbulent velocity $v_{tur} \simeq 3.5$ km s^{-1} in the torus (P04). The HVG has been modeled as gas condensations (see the text). The axis on the left shows the angular offset with respect to the position of the source. On the right, we have included the PSF of the telescope to allow comparisons with the model.

The model adopted to interpret the TEXES/IRTF observations is a modified version of that developed by F08. Although the innermost CSE displays roughly axial symmetry, as several interferometric observations established (Sánchez-Contreras & Sahai 2004; Sánchez-Contreras et al. 2004), we have assumed spherically symmetric abundance distributions for the considered species as a first approximation. This is a reasonable approach since the shells near the central source should not be significantly affected by the outflows. The CSE has been divided in four regions ($\mathcal{Z}_1, \ldots, \mathcal{Z}_4$) related to the torus and the AGB–CSE (see Figure 4). We have assumed a gas density profile $\propto r^{-2}v_{exp}^{-1}$ (constant mass-loss rate), excitation temperature profiles (vibrational and rotational) $\propto r^{-\alpha}$, with α depending on the region, and initially a constant turbulence velocity of 3.5 km s^{-1} in the torus (Pardo et al. 2004). We have added three gas condensations in the inner boundary of region $\mathcal{Z}_1$ with different physical and chemical conditions with respect to the innermost CSE in order to model an inhomogeneous HVG. The synthetic molecular lines have also been fit to the observed ones by eye. This strategy allow us to fit lines partially overlapped with unknown features or affected by irregular baselines impossible to be removed (see Figure 1(b)). The derived parameters are shown in Table 1.

4.1. Uncertainties

We estimated our uncertainties as in F08. Specifically, we explore how the variation of a given parameter affects either the continuum or a molecular line, depending on the nature of the parameter. When using a molecular line, we choose the one most sensitive to the variation of the parameter. We consider a synthetic continuum/line as a good fit to the observed one when all its points deviate from those of the best fit in less than 10% of the maximum absorption when modeling a molecular line and the maximum emission when modeling the continuum. Otherwise, the synthetic spectrum is considered a bad fit. The minimum and maximum values allowed for a given parameter are the smaller and larger of its values which produce good

fits when varying, at the same time, all the other parameters. Therefore, the lower and upper uncertainties are the differences between the minimum and maximum values and that derived from the best fit.

In this work, we have fixed two parameters that cannot be estimated from our observations at the same time as the rest: the distance to CRL618, D, and the angular radius of the central source, α_c. To date, these parameters are not well known, specially D, which could be two times larger (see Section 1).

A variation in any of these parameters affects the linear radius of the central source. An increase in the $\alpha_c D$ product would raise the optical depth ($\tau_\nu \propto \alpha_c D$) diminishing the escape probability of the infrared photons that come from the the inner shells of the torus. This effect could be counteracted by decreasing the column density of the considered molecular species and the dust up to a factor $\simeq$2–3 in our case.

In addition, a variation in α_c would have an impact on the temperature profiles as well. The most affected parameters would be the exponents while the temperatures at the inner boundary of the torus would require minor corrections to recover the best fit.

The approximations adopted to estimate the dipole moments of the rovibrational transitions of C_4H_2, C_6H_2, and C_8H_2 also introduce additional uncertainties in several parameters. The dipole moment of a rovibrational transition behaves as a second degree polynomial on $J(J+1)$ (see, e.g., Jacquemart et al. 2001), while we have assumed that all the rovibrational transitions in a band have the same dipole moment. This different dependence on J alters the derived column densities and excitation temperatures from the real ones. Adopting a maximum deviation of 10% for the (constant) dipole moment squared used in our model with respect to the real one (as occurs for C_2H_2; Jacquemart et al. 2001), the derived column densities and excitation temperatures would be affected by an additional error up to 30%.

Similar variations in the uncertainties of the vibrational temperatures could occur due to having assumed no differences between the vibrational dipole moments of the fundamental band and the associated hot bands.

5. RESULTS AND DISCUSSION

The fits indicate that the deepest absorptions of all lines (Figure 3) have velocities $\simeq -3.5$, -9.0, and $-16.0\,\mathrm{km\,s^{-1}}$, and come from regions $\mathcal{Z}_1$, $\mathcal{Z}_2$, and $\mathcal{Z}_3$, respectively. This is compatible with an expansion velocity profile in which $v_{\rm exp}(R_c) = 1.0$, $v_{\rm exp}(R_{d1}) = 8.0$, $v_{\rm exp}(R_{d2}) = 17.0$, and $v_{\rm exp}(r \gtrsim R_{d3}) = 18.5\,\mathrm{km\,s^{-1}}$. The line C_2H_2 $\nu_5 R_e(21)$ also displays several features with velocities $\simeq$10.0, 2.3, and $-21.8\,\mathrm{km\,s^{-1}}$, not present in the C_4H_2 lines (Figure 3). They do not arise from the CSE and are not hot bands. This fact supports the existence of C_2H_2 in the HVG and suggests that the abundance of C_4H_2 is negligible in it.

The discrete absorptions found in the C_2H_2 lines (Figure 3) produced by the HVG could be the fingerprints of dense clumps whose outermost layers protect the inner molecular gas from being dissociated by the UV radiation field impinging on them and allow a significantly slower chemical evolution in their cores (Redman et al. 2003). In these circumstances, these clumps must be formed due to (1) an irregular mass loss in the latest phases of the stellar atmosphere ejection (Dyson et al. 1989), or (2) density fluctuations or instabilities in the ionization front (Capriotti 1973; García-Segura & Franco 1996; Williams 1999). As the clumps must be in the HVG and in front of the central source, we estimate that their characteristic size should be $\lesssim 1 R_c$.

We derive a vibrational temperature, $T_{\rm vib}$, $\simeq$350 K for C_2H_2 in the innermost CSE and in the HVG. In the CSE, it decreases to $\simeq$200 K between R_c and R_{d1} reaching $\simeq$50–100 K at R_{d3}. For C_4H_2, $T_{\rm vib} \simeq 500$ K in the innermost CSE followed by a fast decrease to $\simeq$400 K at R_{d1} and reaching $\simeq$200–250 K at the end of region $\mathcal{Z}_3$. It is not possible to derive a reliable $T_{\rm vib}$ for C_6H_2 since its lines are very weak but the fits support values similar to that of C_4H_2. The HCN lines do not allow an accurate $T_{\rm vib}$ determination in the torus or in the HVG because of its low abundance. However, the lack of absorption from the hot bands and emission from the fundamental band implies $T_{\rm vib} \lesssim 100$ K. The difference in $T_{\rm vib}$ between HCN, C_2H_2, and C_4H_2 is likely produced by different pumping mechanisms between these species. In particular, we note that some of the hot bands arise from metastable vibrational states (i.e., infrared-inactive).

The synthetic spectra show that the C_2H_2 and C_4H_2 hot bands require lower turbulence velocities ($\lesssim 2\,\mathrm{km\,s^{-1}}$) than fundamental bands ($\simeq 3.5\,\mathrm{km\,s^{-1}}$). It suggests that the turbulence velocity would be lower in regions $\mathcal{Z}_1$ and $\mathcal{Z}_2$, where most of the hot bands arise, than in the rest of the torus. We would need additional observations with a higher signal-to-noise ratio and a more realistic model to explain this result.

Concerning the rotational temperatures, $T_{\rm rot}$, we derive $T_{\rm rot} \simeq 200$ K for C_2H_2. This value has little error because the observed lines are very sensitive to variations in $T_{\rm rot}$. For C_4H_2, we derive $T_{\rm rot} \simeq 100$ K also accurately due to the large number of observed lines. In the case of HCN, $T_{\rm rot} \simeq 350$ K but this time the uncertainties are large since we have only observed two weak lines. The diversity of rotational temperatures indicate that these species are out of local thermal equilibrium (LTE), at least in regions $\mathcal{Z}_1$ and $\mathcal{Z}_2$, which dominate the molecular absorption.

The results support a 3:1 ortho–para ratio for the polyacetylenes, i.e., the ratio expected under LTE conditions. This fact implies that the formation of polyacetylenes occurs in warm regions as suggested in previous works (e.g., C01b; C04), where the ortho–para ratio of the new molecules is given by the spin degeneracy. Taking into account that the rotational constants of the polyacetylenes are small compared to the kinetic temperatures prevailing in the emitting regions, we do not expect ortho–para conversions even though they are not strictly forbidden, contrary to the case of H_2 at low temperatures (Herzberg 1963). Moreover, our result also points out that other processes capable of producing ortho–para conversions such as (1) proton exchange with atomic hydrogen, (2) collisions with paramagnetic molecules or ions such as H^+, H_2^+, or H_3^+, and (3) spin inversion processes on the dust grain surfaces (Farkas 1935; Herzberg 1963; Massie & Hunten 1982; Burton et al. 1992) are inefficient in the innermost CSE.

The C_2H_2 column density in the CSE is $\simeq 2.0 \times 10^{17}\,\mathrm{cm^{-2}}$ coming 45% from the region $\mathcal{Z}_1$, 30% from $\mathcal{Z}_2$, and 25% from $\mathcal{Z}_3$. The contribution from the AGB–CSE (region $\mathcal{Z}_4$) is negligible. The averaged column density in the HVG is $\simeq 1.1 \times 10^{17}\,\mathrm{cm^{-2}}$. Hence, the total column density is $\simeq 3.1 \times 10^{17}\,\mathrm{cm^{-2}}$, in good agreement with $2 \times 10^{17}\,\mathrm{cm^{-2}}$, the value derived by C01b from their low spectral resolution SWS/*ISO* observations (see Table 1 for an error estimation). In addition, the column density that we propose for the CSE agrees with results of the time-dependent chemical models developed by Woods et al. (2002, 2003), which bracket it in the range $\simeq 5 \times 10^{16}$–$5 \times 10^{18}\,\mathrm{cm^{-2}}$, depending on the evolution degree of the envelope. It is possible

to estimate the C_2H_2 abundance ratio between the clumps expanding in the HVG and the gas in the innermost CSE and to compare this result with those of Redman et al. (2003). Assuming a characteristic length in the line of sight $\lesssim 0.5\ R_c$, the averaged gas density in the clumps is $\gtrsim 100\,\mathrm{cm}^{-3}$. Hence, as the C_2H_2 density in the innermost CSE is $\simeq 300\,\mathrm{cm}^{-3}$, the ratio is $\gtrsim 0.3$. Following the results by Redman et al. (2003), this lower limit in the ratio would be achieved after $\simeq 1100$ yr of evolution. However, the age of CRL618 as a PPN has been estimated in several hundreds of years (e.g., Kwok & Bignell 1984).

The C_4H_2 column density in the CSE is $\simeq 2.1 \times 10^{17}\,\mathrm{cm}^{-2}$ (35% from the region $\mathcal{Z}_1$, 60% from $\mathcal{Z}_2$, and 5% from $\mathcal{Z}_3$), again with insignificant contribution from the AGB–CSE (Table 1). As we do not see C_4H_2 in the HVG, the total column density is that derived for the CSE which is a factor $\simeq 2$ larger than $1.2 \times 10^{17}\,\mathrm{cm}^{-2}$, suggested by C01b. The difference between both values is probably due to the large point-spread function (PSF) of *ISO* compared to that of IRTF ($\simeq 3''$ and $0''.7$ at $\simeq 8\ \mu$m, respectively). In this case, our result is very similar to $2.3 \times 10^{17}\,\mathrm{cm}^{-2}$, the maximum abundance for C_4H_2 according to the model of W03 for the evolution of the CSE. As the abundance of C_4H_2 in the HVG is much lower than in the innermost CSE, we estimate the C_4H_2 abundance ratio between the clumps and the innermost CSE in a factor $\lesssim 0.1$. This upper limit supports the results by Redman et al. (2003), which suggest a ratio $\simeq 0.01$–0.3 for clumps aged between 100 and 1000 yr. This period of time and that derived from the C_2H_2 results suggest that a faster chemistry could be needed to better reproduce our results. However, the discrepancies between their results and ours could have to do with differences in the gas density, directly related to the adopted distance to the star, or different simplifications regarding the detailed physical structure of PPN (see more complex models in Pardo et al. 2004; Sánchez-Contreras & Sahai 2004).

For C_6H_2, the column density in the CSE is $\simeq 9.3 \times 10^{16}\,\mathrm{cm}^{-2}$ (15% from the region $\mathcal{Z}_1$ and 85% from $\mathcal{Z}_2$; see Table 1). There is no detectable contribution to the observed C_6H_2 lines from the region $\mathcal{Z}_3$ and from the HVG. Hence, the total column density is in good agreement with the value of $6 \times 10^{16}\,\mathrm{cm}^{-2}$, derived by C01b. The maximum column density proposed by W03 ($\simeq 7.7 \times 10^{16}\,\mathrm{cm}^{-1}$) is similar to our result but somewhat lower. It might indicate that the model developed by these authors needs to be slightly improved as far as the interaction between polyacetylenes and dust grains or unconsidered chemical reactions involving polyacetylenes are concerned.

Finally, the column density of HCN in the CSE is $\simeq 2.0 \times 10^{17}\,\mathrm{cm}^{-2}$ and the averaged column density in the HVG is $\simeq 5.0 \times 10^{16}\,\mathrm{cm}^{-2}$. Both results are affected by a large error due to the weakness of the observed lines. Hence, we can conclude that the total column density is $\simeq 2.5 \times 10^{17}\,\mathrm{cm}^{-2}$ (Table 1), in good agreement with $1.5 \times 10^{17}\,\mathrm{cm}^{-2}$ proposed by C01b but smaller than the value of $\simeq 4$–$7 \times 10^{17}\,\mathrm{cm}^{-2}$, derived by Pardo et al. (2004, 2005). The discrepancy existing with the latter result can be attributed to HCN molecules known to exist in the cold region $\mathcal{Z}_4$ (AGB–CSE), unobserved through infrared observations. As in the case of C_4H_2, the maximum column density expected by W03 is similar but larger than that derived by us, suggesting that their model works also fine for HCN.

The abundance of C_8H_2 estimated from the results by C01b and that proposed by W03 and C04 suggests that the C_8H_2 $\nu_{10} + \nu_{14}$ band should be observed in our spectrum. Nevertheless, we have not found any pattern of lines that could be assigned to this species. The telluric contributions to the raw spectra of CRL618 were removed by dividing the latter by the corresponding spectra of the BN object, free of intrinsic molecular lines in the observed frequency range. Further corrections were performed to mend minor instrumental features from the spectra. Therefore, we are sure that we did not accidentally remove any broad feature such as the C_8H_2 band. The upper limit to its total column density, calculated by assuming a peak intensity for the $\nu_{10} + \nu_{14}$ band lower than 10% the continuum, and the same excitation temperatures and coexisting with C_6H_2, is $5 \times 10^{16}\,\mathrm{cm}^{-2}$. This value is lower than the column densities of C_2H_2, C_4H_2, and C_6H_2 in the CSE by a factor 4.0, 4.2, and 1.9, respectively.

The abundance ratio $[C_2H_2]/[C_4H_2]$ in the torus is $\simeq 0.95$, compatible with a region where the abundances have reached the steady state (C04). The abundance ratios in each region ($\mathcal{Z}_1$, $\mathcal{Z}_2$, and $\mathcal{Z}_3$) are 1.2, 0.49, and 3.5, respectively. The abundances in $\mathcal{Z}_1$ seem to be in steady state while in $\mathcal{Z}_3$ they are still evolving. In the region $\mathcal{Z}_2$, the ratio is very low indicating variations in the abundances, likely related to condensation onto dust grains or involvement in chemical reactions still unconsidered in the current chemical models. The ratio $[C_4H_2]/[C_6H_2] \simeq 2.3$, in good agreement with the results suggested by C04 for evolving abundances. The C_6H_2 lines are too weak to derive reliable ratios for each region in the torus.

5.1. SMP LMC 11, CRL618, and IRC+10216

The PPN SMP LMC 11, located in the Large Magellanic Cloud (LMC), is known to display several bands in absorption arising from C_2H_2, C_4H_2, and C_6H_2 (Bernard-Salas et al. 2006 and references therein). This fact suggests that the chemistry in its CSE is very similar to that in CRL618. Hence, a comparison between these two sources could contribute interesting clues to a future chemical model of SMP LMC 11.

The observations carried out in the infrared by Bernard-Salas et al. (2006) toward SMP LMC 11 show a wide absorption in the continuum ranging from 12 to 17 μm, formed by the blending of several hundreds of lines of C_2H_2, C_4H_2, C_6H_2, and other abundant molecules such as C_6H_6. From this feature, it can be inferred that C_2H_2 is more abundant than in CRL618, even as much as in IRC+10216 (with a column density $\simeq 1.6 \times 10^{19}\,\mathrm{cm}^{-2}$; F08), where a broad absorption at $\simeq 13\ \mu$m was also observed (Cernicharo et al. 1999). The presence of strong hot bands such as $\nu_4 + \nu_5 - \nu_5$, $2\nu_5 - \nu_5$ (at 13.5–14.0 μm), and $\nu_4 + \nu_5$ (at $\simeq 7.5\ \mu$m) in absorption indicates that the vibrational temperature in the innermost CSE should be $\simeq$500–600 K, i.e., between those of CRL618 (with weak hot bands; see Figure 1(a)) and IRC+10216 (with strong hot bands; F08). This excitation would be probably caused by a somewhat strong infrared radiation field produced by the warm dust, as in the case of IRC+10216 (e.g., F08).

Concerning the rest of the polyacetylenes, the lower abundance ratio between C_6H_2 and C_4H_2 in SMP LMC 11 than in CRL618 suggest that the former source is chemically less evolved than the latter (W03; C04), in agreement with Bernard-Salas et al. (2006). To date, it has been impossible to clearly detect C_8H_2 toward CRL618. However, the great resemblance in their chemistry and the good agreement between observations and chemical models suggest that C_8H_2 could be built up from C_6H_2 in the CSE of both sources. Bernard-Salas et al. (2006) compare, in their Figure 2, two low-resolution mid-infrared spectra of CRL618 and SMP LMC 11. These spectra seem to share a weak unidentified feature at $\simeq 16\ \mu$m, between the bands

ν_8 and ν_{11} of C_4H_2 and C_6H_2, respectively. This feature could be the Q branch of the C_8H_2 band ν_{14}, several times stronger than $\nu_{10} + \nu_{14}$ at room temperature (Shindo et al. 2001). It should be observed in the future with higher spectral resolution to assess whether it can be assigned to the ν_{14} band of C_8H_2. The recent discovery of C_{60} and C_{70} (Cami et al. 2010) strongly support the growth mechanism for carbon clusters proposed by C04. In his models, carbon clusters were produced from the photodissociation of polyacetylenes and, although limited to C_{18}, the predicted abundances for these large carbon species are very large.

6. SUMMARY AND CONCLUSIONS

In this paper, we present high-resolution mid-infrared observations toward the PPN CRL618. The sampled spectral ranges (778–784 and 1227–1249 cm^{-1}) observed with the high resolving power spectrograph TEXES allow us to resolve bands $\nu_6+\nu_8$ and $\nu_8 + \nu_{11}$ of C_4H_2 and C_6H_2, respectively, in addition to several lines of bands ν_5 and ν_2 of C_2H_2 and HCN. These rich data have enabled the modeling of the useful rovibrational line profiles of these molecular species to estimate their abundances and the physical conditions of the gas and the dust throughout the inner CSE.

The analysis of the observations has yielded the following results, among others.

1. Our results support the chemical model suggested by W03 and C04 for the polymerization of C_2H_2.
2. Most of the HCN and C_2H_2 are in the inner CSE. The rest come from several dense clumps located in the HVG.
3. C_4H_2 and C_6H_2 are formed in the innermost CSE. Their abundances seem to be negligible in the clumps since the emission from these molecules is undetectable in our spectrum.
4. We are not able to detect any trace of the C_8H_2 band $\nu_{10}+\nu_{14}$, expected to fall in the observed range. This implies an even lower abundance for this species compared to previously suggested values. An upper limit to its column density has been estimated.
5. There exist large differences between the excitation temperatures (vibrational and rotational) of HCN, C_2H_2, and C_4H_2 which indicate that the inner CSE is out of LTE.

In addition, the results of this work demonstrate the power of IR observations in the determination of the abundances and physical conditions of the gas in complex structured environments such as the innermost envelopes of the evolved stars. Further improvements in the search for C_8H_2 will be made in the future by observing CRL618 and SMP LMC 11 at $\simeq$16 μm with the Echelon-cross-Echelle Spectrograph (EXES) mounted on the Stratospheric Observatory for Infrared Astronomy (SOFIA).

J.C. and J.P.F. thank the Spanish Ministerio de Educación y Ciencia for funding support through grant ESP2004-665, AYA2003-2785, and the "Comunidad de Madrid" government under PRICIT project S-0505/ESP-0237 (ASTROCAM). This study is supported in part by the European Community's human potential Programme under contract MCRTN-CT-2004-51230, "Molecular Universe." During this study, J.P.F. was supported by the CSIC and the "Fondo Social Europeo" under internship grant from the I3P Programme, by CONACyT under project SEP-2004-C01-47090, and by the UNAM through a postdoctoral fellowship. M.J.R. is supported by grant AST-0708074. TEXES was built with funds from the NSF. We acknowledge the referee for his/her useful comments.

REFERENCES

Arié, E., & Johns, J. W. C. 1992, J. Mol. Spec., 155, 195
Becklin, E. E., & Neugebauer, G. 1967, ApJ, 147, 799
Bernard-Salas, J., Peeters, E., Sloan, G. C., Cami, J., Guiles, S., & Houck, J. R. 2006, ApJ, 652, L29
Burton, M. G., & Geballe, T. R. 1986, MNRAS, 223, 13
Burton, M. G., Hollenbach, D. J., & Tielens, A. G. G. M. 1992, ApJ, 399, 563
Cami, J., Bernard-Salas, J., Peeters, E., & Malek, S. E. 2010, Science, 329, 1180
Capriotti, E. R. 1973, ApJ, 179, 495
Cernicharo, J., Guélin, M., Martín-Pintado, J., Peñalver, J., & Mauersberger, R. 1989, A&A, 222, L1
Cernicharo, J., Heras, A. M., Pardo, J. R., Tielens, A. G. G. M., Guélin, M., Dartois, E., Neri, R., & Waters, L. B. F. M. 2001b, ApJ, 546, L127
Cernicharo, J., Heras, A. M., Tielens, A. G. G. M., Pardo, J. R., Herpin, F., Guélin, M., & Waters, L. B. F. M. 2001a, ApJ, 546, L123 (C01b)
Cernicharo, J., Yamamura, I., González-Alfonso, E., de Jong, T., Heras, A., Escribano, R., & Ortigoso, J. 1999, ApJ, 526, L41
Cernicharo, J. 2004, ApJ, 608, L41 (C04)
Dyson, J. E., Hartquist, T. W., Pettini, M., & Smith, L. J. 1989, MNRAS, 241, 625
Farkas, A. 1935, Orthohydrogen, Parahydrogen, and Heavy Hydrogen (Cambridge: Cambridge Univ. Press)
Foing, B. H., & Ehrenfreund, P. 1994, Nature, 369, 296
Fonfría, J. P., et al. 2008, ApJ, 673, 445 (F08)
Fuente, A., Cernicharo, J., & Omont, A. 1998, A&A, 330, 232
Gammie, C. F., Knapp, G. R., Young, K., Phillips, T. G., & Falgarone, E. 1989, ApJ, 345, L87
García-Segura, G., & Franco, J. 1996, ApJ, 469, 171
García-Hernández, D. A., Manchado, A., García-Lario, P., Stanghellini, L., Villaver, E., Shaw, R. A., Szczerba, R., & Perea-Calderón, J. V. 2010, ApJ, 724, L39
Goodrich, R. W. 1991, ApJ, 376, 654
Guelachvili, G., Craig, A. M., & Ramsay, D. A. 1984, J. Mol. Spec., 105, 156
Haas, S., Yamada, K. M. T., & Winnewisser, G. 1994, J. Mol. Spec., 164, 445
Herpin, F., & Cernicharo, J. 2000, ApJ, 530, L129
Herzberg, G. 1963, Molecular Spectra and Molecular Structure. I. Spectra of Diatomic Molecules (Princeton, NJ: Van Nostrand)
Hony, S., Waters, L. B. F. M., & Tielens, A. G. G. M. 2002, A&A, 390, 533
Iben, I., & Renzini, A. 1983, ARA&A, 21, 271
Jacquemart, D., Claveau, C., Mandin, J.-Y., & Dana, V. 2001, J. Quant. Spectrosc. Radiat. Transfer, 69, 81
Khlifi, M., Paillous, P., Delpech, C., Nishio, M., Bruston, P., & Raulin, F. 1995, J. Mol. Spec., 174, 116
Kleinmann, S. G., Sargent, D. G., Moseley, H., Harper, D. A., Loewenstein, R. F., Telesco, C. M., & Thronson, Jr., H. A. 1978, A&A, 65, 139
Knapp, G. R., & Morris, M. 1985, ApJ, 292, 640
Knapp, G. R., Sandell, G., & Robson, E. I. 1993, ApJS, 88, 173
Kwok, S., & Bignell, R. C. 1984, ApJ, 276, 544
Kwok, S., Purton, C. R., & Fitzgerald, P. M. 1978, ApJ, 219, L125
Lacy, J. H., Richter, M. J., Greathouse, T. K., Jaffe, D. T., & Zhu, Q. 2002, PASP, 114, 153
Massie, S. T., & Hunten, D. M. 1982, Icarus, 49, 213
Matsumura, K., & Tanaka, T. 1982, J. Mol. Spec., 96, 219
Matsumura, K., & Tanaka, T. 1984, J. Mol. Spec., 108, 299
Matsumura, K., Kawaguchi, K., McNaughton, D., & Bruget, D. N. 1993, J. Mol. Spec., 158, 489
McNaughton, D., & Bruget, D. N. 1991, J. Mol. Spec., 150, 620
McNaughton, D., & Bruget, D. N. 1992, J. Mol. Struct., 273, 11
Pardo, J. R., Cernicharo, J., & Goicoechea, J. R. 2005, ApJ, 628, 275
Pardo, J. R., Cernicharo, J., Goicoechea, J. R., & Phillips, T. G. 2004, ApJ, 615, 495 (P04)
Pardo, J. R., & Cernicharo, J. 2007, ApJ, 654, 978
Pardo, J. R., et al. 2007, ApJ, 661, 250
Pottasch, S. R. 1984, Planetary Nebulae—A Study of Late Stages of Stellar Evolution (Astrophys. Space Sci. Lib. 107; Dordrecht: Reidel)
Redman, M. P., Viti, S., Cau, P., & Williams, D. A. 2003, MNRAS, 345, 1291
Remijan, A. J., Wyrowski, F., Friedel, D. N., Meier, D. S., & Snyder, L. E. 2005, ApJ, 626, 233
Rothman, L. S., et al. 2005, J. Quant. Spectrosc. Radiat. Transfer, 96, 139
Rouleau, F., & Martin, P. G. 1991, ApJ, 377, 526
Sánchez-Contreras, C., Bujarrabal, V., Castro-Carrizo, A., Alcolea, J., & Sargent, A. 2004, ApJ, 617, 1142

Sánchez-Contreras, C., & Sahai, R. 2004, ApJ, 602, 960
Schmidt, G. D., & Cohen, M. 1981, ApJ, 246, 444
Sellgren, K., Werner, M. W., Ingalls, J. G., Smith, J. D. T., Carleton, T. M., & Joblin, C. 2010, ApJ, 722, L54
Shindo, F., Bénilan, Y., Chaquin, P., Guillemin, J.-C., Jolly, A., & Raulin, Fr. 2001, J. Mol. Spec., 210, 191
Shindo, F., Benilan, Y., Guillemin, J.-C., Chaquin, P., Jolly, A., & Raulin, F. 2003, Planet. Space Sci., 51, 9
Sopka, R. J., Hildebrand, R., Jaffe, D. T., Gatley, I., Roellig, T., Werner, M., Jura, M., & Zuckerman, B. 1985, ApJ, 294, 242
Trammell, S. R. 2000, in ASP Conf. Ser.199, Asymmetrical Planetary Nebulae II: From Origins to Microstructures, ed. J. H. Kastner, N. Soker, & S. Rappaport (San Francisco, CA: ASP), 147
Truong-Bach , Graham, D., & Nguyen-Q-Rieu, 1996, A&A, 312, 565
Westbrook, W. E., Becklin, E. E., Merrill, K. M., Neugebauer, G., Schmidt, M., Willner, S. P., & Wynn-Williams, C. G. 1975, ApJ, 202, 407
Williams, R. J. R. 1999, MNRAS, 310, 789
Woods, P. M., Millar, T. J., Herbst, E., & Zijlstra, A. A. 2003, A&A, 402, 189 (W03)
Woods, P. M., Millar, T. J., Zijlstra, A. A., & Herbst, E. 2002, ApJ, 574, L167